Volume 9
Number 18
21 September 2025
Pages 4763–5098

Sustainable Energy & Fuels

Interdisciplinary research for the development of sustainable energy technologies

rsc.li/sustainable-energy

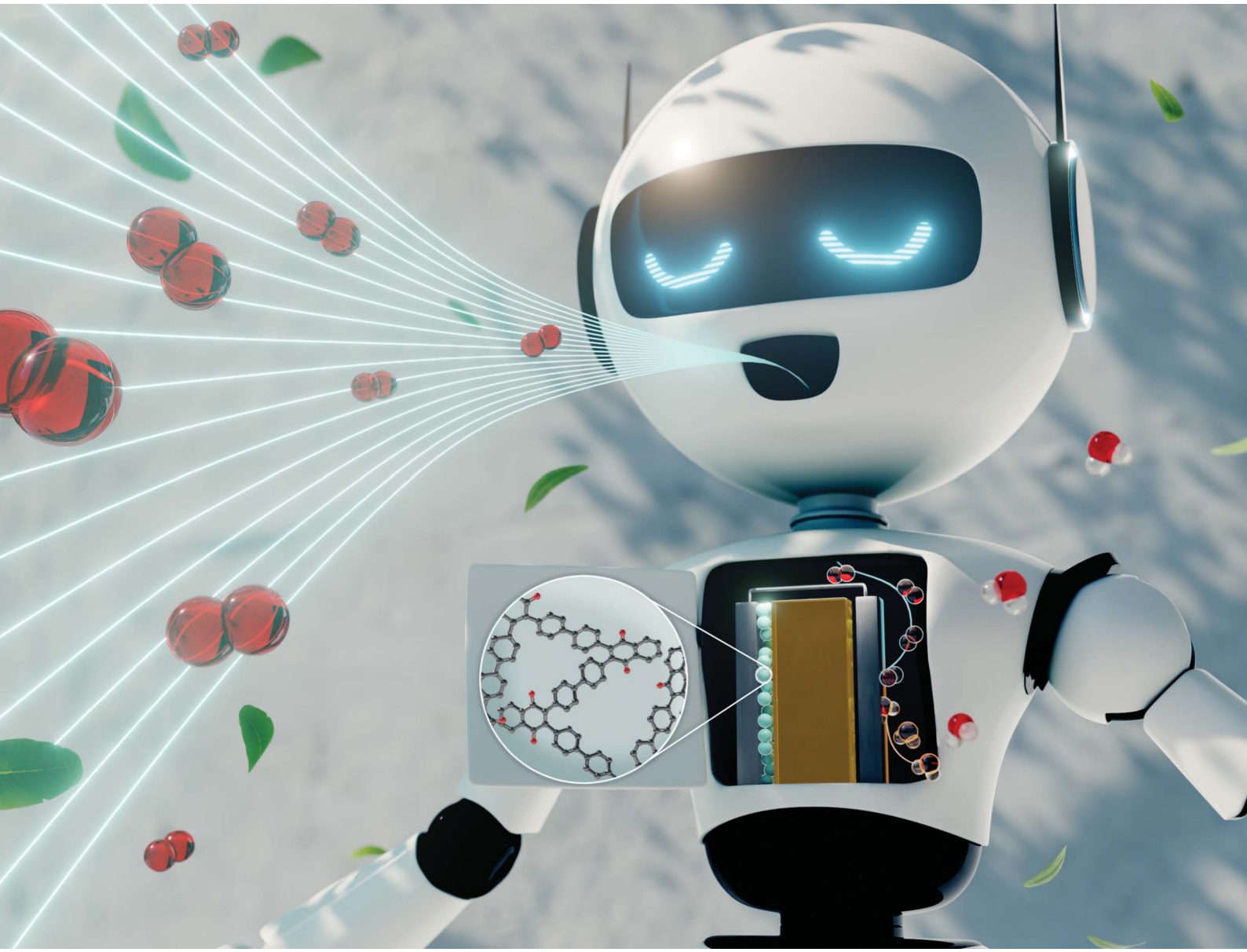

ISSN 2398-4902

ROYAL SOCIETY OF CHEMISTRY

COMMUNICATION

Kenji Miyatake *et al.*

Enhanced performance of all-solid-state rechargeable air batteries with a redox-active naphthoquinone-based polymer electrode

Sustainable Energy & Fuels

ROYAL SOCIETY OF CHEMISTRY

COMMUNICATION

View Article Online
View Journal | View Issue

Cite this: *Sustainable Energy Fuels*, 2025, 9, 4882

Received 13th June 2025
Accepted 24th July 2025

DOI: 10.1039/d5se00825e

rsc.li/sustainable-energy

Enhanced performance of all-solid-state rechargeable air batteries with a redox-active naphthoquinone-based polymer electrode†

Lin Guo, [a] Kenji Miyatake, *[abc] Fang Xian,[a] Fanghua Liu,[a] Ahmed Mohamed Ahmed Mahmoud,[a] Vikrant Yadav[a] and Chun Yik Wong[a]

All-solid-state rechargeable air batteries (SSABs) have emerged as a promising next-generation battery technology, eliminating the need for liquid electrolytes and reducing the reliance on metal-based electrode materials, while mitigating bulky design issues such as excessive mass and size. Herein, we propose an SSAB that uses a novel redox-active polymer containing a naphthoquinone moiety (PPNQ) as the negative electrode material and evaluate its electrochemical performance. The SSAB-PPNQ cell exhibited superior rate capability and charge/discharge cycle stability compared to SSABs utilizing small organic molecules, owing to the enhanced structural stability and redox reversibility of PPNQ. The reduced dissolution and/or possible degradation during repeated charge/discharge cycles enhanced the rate properties (84% retention of its discharge capacity at 100C) and cyclability (98% retention of its charge/discharge capacities over 100 cycles) of the SSAB-PPNQ cell, highlighting the potential of the PPNQ redox-active polymer as a promising candidate for high-performance SSABs.

With increasing demand for sustainable and high-performance energy storage systems, organic electrode materials have emerged as promising candidates for secondary batteries due to their environmental benignity, structural diversity, and tunable redox properties. In particular, organic air batteries, which utilize redox-active organic molecules as the negative electrode material and ambient air as the positive reactant, offer great potential for light-weight, cost-effective, and eco-friendly energy storage devices.[1–3] Compared to conventional metal–air batteries which employ metal-based (Li, Na, Zn, *etc.*) negative electrodes, the use of organic-based negative electrodes avoids issues such as dendrite formation and parasitic side reactions, while providing greater molecular design flexibility, redox reversibility, and water stability.[4–6] For example, a π-conjugated *N*-heteroaromatic phenazine derivative (NHCC) was previously used as the active negative electrode material in an organic–air battery, exhibiting a high cell voltage of 1.6 V and lifetime of 30 000 charge/discharge cycles when coupled with aqueous electrolyte (4 M KOH and 10 M KCF_3SO_3).[7] Additionally, an air battery using 1,8-dihydroxyanthraquinone-substituted poly(-allyl amine) (PDHA) as the negative electrode material and aqueous H_2SO_4 as the electrolyte exhibited a discharge capacity of 140 mAh g^{-1}, with excellent cyclability (>97% retention of its discharge capacity over 500 charge/discharge cycles) and a high rate capability up to 120 °C.[8] A redox-active donor–acceptor conjugated microporous polymer (AQ-CMP) containing anthraquinone and benzene served as the negative electrode in an air battery which demonstrated a specific capacity of 202 mAh g^{-1} (96% of theoretical capacity) at 2 A g^{-1}, excellent rate capability (58% capacity retention at 20 A g^{-1}), and *ca.* 100% capacity retention over 60 000 charge/discharge cycles in 6 M KOH solution.[9] Despite the encouraging results, the use of liquid electrolytes provided these organic–air batteries with some drawbacks such as electrolyte leakage, increased weight, and limited compatibility with miniaturized or flexible devices. To overcome these limitations, a combination of solid polymer electrolyte with organic negative electrodes seems a promising direction, particularly for next-generation compact energy storage systems.

We recently developed organic SSABs using 2,5-dihydroxy-1,4-benzoquinone (DHBQ) or its polymeric counterpart, poly(2,5-dihydroxy-1,4-benzoquinone-3,6-methylene) (PDBM), as the negative electrode material and a proton-conductive Nafion™ membrane as the solid electrolyte.[10] The batteries were operable with an open circuit voltage (OCV) of 0.80 V. Notably, the SSAB-PDBM cell achieved a higher discharge capacity (176.1 mAh g^{-1}) than the SSAB-DHBQ cell (29.7 mAh g^{-1}) and retained 78% of its capacity over 30 charge/discharge cycles, highlighting the promising potential of polymeric redox-active molecules in SSABs. More recently, we fabricated

[a]*Clean Energy Research Center, University of Yamanashi, Kofu, Yamanashi 400-8510, Japan. E-mail: miyatake@yamanashi.ac.jp*

[b]*Hydrogen and Fuel Cell Nanomaterials Center, University of Yamanashi, Kofu, Yamanashi 400-8510, Japan*

[c]*Department of Applied Chemistry, Waseda University, Tokyo 169-8555, Japan*

† Electronic supplementary information (ESI) available. See DOI: https://doi.org/10.1039/d5se00825e

an SSAB using 1,4-naphthoquinone (NQ) as the negative electrode material and a less gas-permeable aromatic ionomer-based proton-conductive membrane (SPP-QP) as the solid electrolyte.[11] The SPP-QP membrane, with an ion exchange capacity (IEC) of 3.1 mmol g^{-1}, exhibited proton conductivities of 0.157 S cm^{-1} at 80 °C and 0.077 S cm^{-1} at 40 °C at 80% relative humidity (RH) (Fig. S1†), both of which were higher than those of the commercial Nafion 212 membrane (0.100 S cm^{-1} at 80 °C and 0.066 S cm^{-1} at 40 °C). The results indicate that the SPP-QP membrane possesses sufficient proton conductivity to support effective proton transport in the SSAB configuration. The SSAB-NQ cell exhibited an OCV of 1.06 V and prolonged charge/discharge cyclability, retaining 88% of its capacity over 100 charge/discharge cycles and >98% of its coulombic efficiency (CE) over 135 cycles. These results prompted us to design a novel redox-active polymer containing an NQ moiety (PPNQ) as the negative electrode material in SSABs. In the present study, the synthesis, electrochemical properties, and SSAB performance of PPNQ were investigated and compared to those of our previously reported SSABs.

The DPNQ monomer was synthesized through the bromination of NQ, followed by a reaction with 4-chlorophenylboronic acid *via* the Pd(0)-catalyzed cross-coupling reaction (Fig. 1a) in a total yield of 47%. The chemical structures of DBNQ and DPNQ were confirmed using ^{1}H and ^{13}C nuclear magnetic resonance (NMR) spectra (Fig. 1b and c). The PPNQ polymer was then synthesized through the polymerization of the DPNQ monomer *via* the Ni(0)-mediated polycondensation reaction, whose structure was also confirmed using the ^{1}H NMR spectrum (Fig. 1d). The resulting PPNQ polymer was soluble in *N*,*N*-dimethylformamide (DMF), *N*,*N*-dimethylacetamide (DMAc), and dimethyl sulfoxide (DMSO). The molecular weight of the PPNQ was M_w = 3.26 kDa and M_n = 2.20 kDa with a narrow polydispersity index (M_w/M_n = 1.49).

A catalyst-coated membrane (CCM) containing platinum/carbon (Pt/C) as the positive electrode catalyst and PPNQ as the redox-active negative electrode material was prepared and assembled into a cell (see the ESI† for details). The cross-sectional scanning electron microscopy (SEM) images of the freshly prepared CCM are shown in Fig. S2a–c.† The positive and negative electrode inks were uniformly sprayed onto both sides of the SPP-QP membrane (*ca.* 60 μm-thick), forming consistent electrode layers with thicknesses of *ca.* 20 and 100 μm, respectively. No significant aggregated clusters were observed in the magnified images of electrodes, indicating the successful fabrication of a uniform CCM. Sulfur intensity in the EDS analysis (Fig. S2g†) as a measure of the sulfonic acid group density revealed that the sulfonic acid content in the SPP-QP membrane (*ca.* 85%) was more than four times higher than that in the negative electrode layer (*ca.* 20%). The lower sulfonic acid density combined with the greater thickness of the negative electrode layer suggests that proton transport was probably limited within the negative electrode compared to that in the SPP-QP membrane. Prior to charging and discharging the SSAB, the cyclic voltammetry (CV) curve of the negative electrode was measured at 80% RH. Compared to the CV curve of the monomeric NQ-based negative electrode reported in our previous paper, which exhibited major redox peaks at *ca.* 0.40 and 0.48 V with minor peaks at 0.28 and 0.52 V, the SSAB-PPNQ cell displayed a single set of distinct redox peaks at 0.46 and 0.31 V (Fig. 1e). The results suggested the occurrence of a one-step two-electron transfer process during the hydroquinone/quinone redox reaction in PPNQ. NQ utilization in the SSAB-PPNQ cell (based on the charge of the reduction peak divided by the number of moles of the NQ moiety in PPNQ loaded in the electrode, assuming a two-electron redox reaction) was calculated to be 17.0%, which was slightly higher than that in the SSAB-NQ cell (16.5%, measured at 100% RH). The improved NQ utilization in the SSAB-PPNQ cell compared to the SSAB-NQ cell indicated that the affinity of polymeric PPNQ for the hydrophilic proton-conducting polymer (Nafion™) was potentially better than that of monomeric NQ. Similar results were obtained with DHBQ. Additionally, the CV curve of the PPNQ negative material was measured in an aqueous acidic solution (0.05 M sulfuric acid) at room temperature as shown in Fig. S3.† Distinct redox peaks were observed at 0.41 and 0.38 V with a narrow potential separation of 0.03 V compared to 0.15 V observed in the SSAB. The results indicate a more reversible redox reaction in the aqueous electrolyte due to the enhanced proton supply. Furthermore, the utilization of NQ in the aqueous electrolyte reached 83.4%, which was more than four times higher than that in the SSAB. The limited proton supply in the solid-state lowered the utilization of the redox-active material in the negative electrode. Electrochemical impedance spectroscopy (EIS) of the SSAB-PPNQ cell was conducted after the CV measurement, and the results are presented as a Nyquist plot in Fig. S4.† The plot exhibited two distinct semicircles in the high- and mid-frequency regions. The small semicircle at high frequency was attributed to the interfacial resistance and contact impedance between the solid electrolyte and the electrodes. The larger semicircle at mid frequency was ascribed to the charge-transfer resistance associated with the proton-coupled redox reactions occurring at both electrodes.

The energy storage mechanism of the SSAB-PPNQ cell involves proton-coupled redox reactions at both electrodes as illustrated in Fig. 1f. During the charging, the PPNQ negative electrode is reduced by accepting two electrons and two protons per quinone unit forming hydroquinone. The protons originated from water splitting at the positive electrode, where water molecules are oxidized to release protons and oxygen. During the discharging, the hydroquinone units in PPNQ are oxidized back to quinone, releasing electrons and protons. Meanwhile, the oxygen at the positive electrode is reduced to water with electrons and protons, completing the redox cycle. The charging/discharging curves of the SSAB-PPNQ cell obtained at a constant current density of 0.23 mA cm^{-2} (at a 3.9C rate) are illustrated in Fig. 2. During charging, the potential of the positive electrode (where the water oxidation reaction occurred to generate oxygen) (Fig. 2a) initially increased from *ca.* 0.97 to 1.05 V and then gradually increased to *ca.* 1.14 V. In the final stage of charging, the potential increased rapidly to *ca.* 1.23 V, which was attributed to the accumulation of oxygen generated on the electrode surface causing mass transport overpotential.[12] The potential of the negative electrode (where PPNQ was

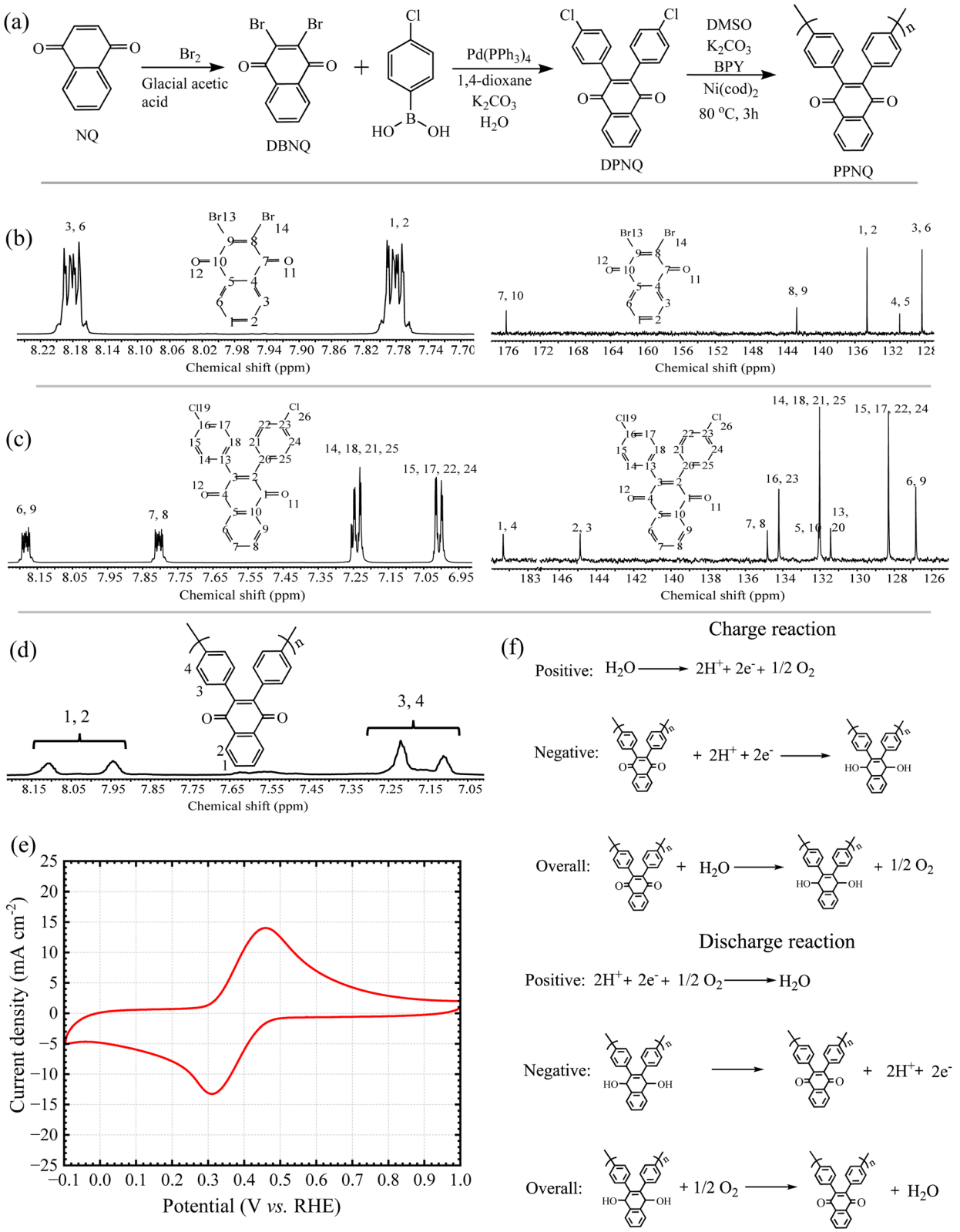

Fig. 1 (a) Synthetic scheme of DBNQ and DPNQ monomers and the PPNQ polymer. ^{1}H (left) and ^{13}C (right) NMR spectra of (b) DBNQ and (c) DPNQ in $CDCl_3$ at room temperature. (d) ^{1}H NMR spectra of the PPNQ polymer in DMSO-d_6 at room temperature. (e) CV curves of the SSAB-PPNQ cell scanned at 20 mV s^{-1} (40 °C and 80% RH) for the negative electrode. (f) Electrode and overall reactions during charging and discharging.

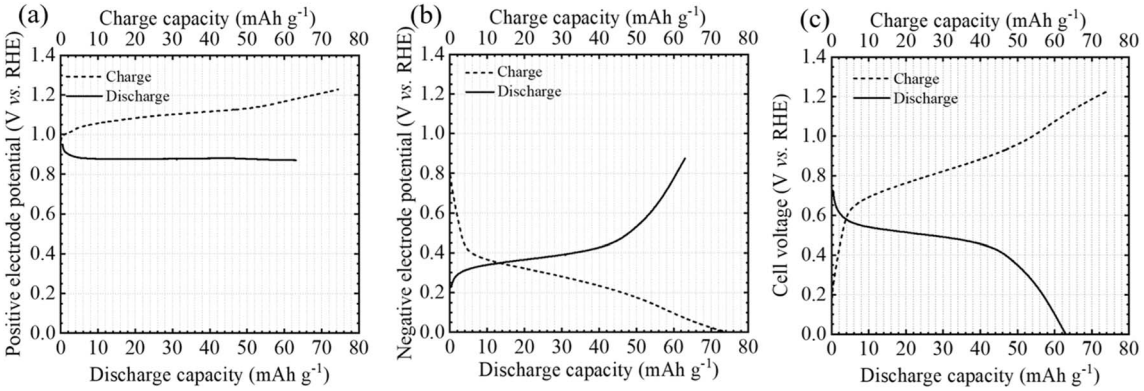

Fig. 2 Charging/discharging curves of the SSAB-PPNQ cell measured at a current density of 0.23 mA cm^{-2}: (a) positive electrode potential, (b) negative electrode potential, and (c) cell voltage.

reduced) (Fig. 2b) rapidly decreased from *ca.* 0.79 to 0.40 V and then gradually decreased to 0 V, at which point charging was terminated to avoid the occurrence of the hydrogen evolution reaction (HER) (or the proton reduction reaction). Accordingly, the cell voltage (Fig. 2c) rapidly increased from *ca.* 0.18 to 0.64 V and then gradually increased to *ca.* 1.23 V, mostly dominated by the negative electrode. The charge capacity was 74.4 mAh g^{-1}, from which the PPNQ utilization was calculated to be 40%, which was 23% higher than that calculated from the CV curve. These results suggested that more PPNQ molecules participated in the redox reaction under dynamic conditions than under static conditions. During discharging, the potential of the positive electrode (where oxygen was reduced to produce water) (Fig. 2a) rapidly decreased from *ca.* 0.95 to 0.88 V and then remained nearly constant until the end of the discharging process, whereas the potential of the negative electrode (where PPNQ was oxidized) initially quickly increased from *ca.* 0.23 to 0.30 V and then gradually increased to *ca.* 0.45 V, followed by another sharp rise to *ca.* 0.88 V (Fig. 2b). The OCV of the SSAB-PPNQ cell (0.73 V) was lower than that of our previous SSABs using DHBQ, NQ, and PE-AQ, an anthraquinone derivative[13] (*ca.* 0.80, 1.10, and 1.10 V, respectively, when operated at 100% RH) (Fig. 2c). The lower OCV of the SSAB-PPNQ cell compared to previous SSABs was mainly attributed to the higher redox potential and the large redox peak separation (or electrochemical irreversibility) of the PPNQ redox reaction, in addition to the lower but more practical RH used in this study compared to the fully humidified conditions adopted in previous studies (80% *vs.* 100% RH). In fact, the OCV of the SSAB-NQ cell decreased to *ca.* 1.05 V when operated at 80% RH. As discharging proceeded, the cell voltage of the SSAB-PPNQ cell rapidly decreased to 0.58 V and then gradually decreased to *ca.* 0.55–0.45 V, presenting a somewhat higher nominal cell voltage (near the plateau cell voltage during discharging) than the SSAB-DHBQ and SSAB-NQ cells (*ca.* 0.50–0.30 and 0.40–0.24 V, respectively) but a lower nominal cell voltage than the SSAB-PE-AQ cell (*ca.* 0.70–0.60 V). Similar to the charging process, the cell voltage during discharging was dominated by the negative electrode. The discharge capacity of the SSAB-PPNQ cell (63.1 mAh g^{-1}) was higher than that of the SSAB-DHBQ cell (29.7 mAh g^{-1}), which was attributed to the instability of the negative electrode, but it was lower than those of the SSAB-NQ and SSAB-PE-AQ cells (83.6 and 99.9 mAh g^{-1}, respectively). Compared to the SSAB-NQ cell, which exhibited a discharge capacity of 50.0 mAh g^{-1} at 80% RH, the SSAB-PPNQ cell was more capacitive. The CE of the SSAB-PPNQ cell (85%) was lower than those of the SSAB-DHBQ, SSAB-NQ, and SSAB-PE-AQ cells (*ca.* 100%, 87% and 100%, respectively), which was presumably caused by the limited redox reactions of PPNQ owing to electrochemical irreversibility under lower humidity (80% RH) conditions. The charging/discharging curves of the SSAB-PPNQ cell at lower constant current densities of 0.06 mA cm^{-2} (1C rate) and 0.03 mA cm^{-2} (0.5C rate) are shown in Fig. S5.† Compared to the performance at 3.9C, the increased charge/discharge capacities (73.5/67.0 mAh g^{-1} at 1C and 81.2/78.7 mAh g^{-1} at 0.5C) and improved CEs (91% at 1C and 97% at 0.5C) indicate that lower C rates effectively improved the proton supply and redox kinetics of PPNQ in the solid-state.

Based on the abovementioned discharge capacity, the C rate was determined. The rate characteristics were evaluated while increasing the discharge rate from 4 to 100C (or a current density from 0.24 to 5.87 mA cm^{-2}), while the charge rate was maintained at 4C. The discharging curves at different C rates are summarized in Fig. 3a–c (see Fig. S6† for the charging curves). The initial positive (Fig. 3a) and negative (Fig. 3b) electrode potentials remained nearly constant at all discharge C rates, at *ca.* 0.92 and 0.20 V, respectively, resulting in the same OCV of *ca.* 0.72 V for the SSAB-PPNQ cell (Fig. 3c). The discharge capacity of the SSAB-PPNQ cell decreased from 68.4 to 57.4 mAh g^{-1} from 4 to 100C, retaining 84% of its discharge capacity at 100C, which was superior to that of the SSAB-NQ cell (79% retention of its discharge capacity when operated at a 100C rate and 100% RH). The final potential (at which discharging was terminated) of the negative electrode decreased from *ca.* 0.77 to 0.72 V from 4 to 100C, retaining 94% of its initial value at 100C. Given that the positive electrode potential of the SSAB-PPNQ, SSAB-NQ, and SSAB-PE-AQ cells exhibited a similar dependence on the discharge rate, the rate characteristics of the discharge capacity were mostly dominated by the negative electrode. The negative electrode potential of the SSAB-NQ cell was initially *ca.* 0.19 V, and

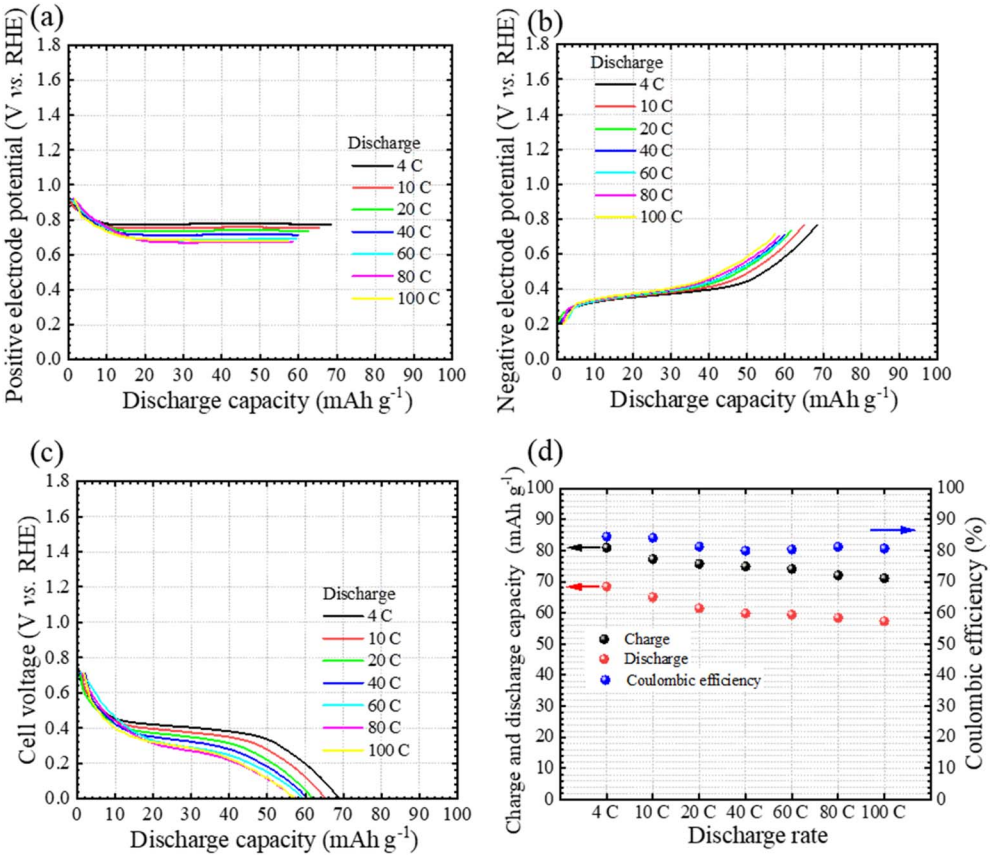

Fig. 3 Discharging curves of the SSAB-PPNQ cell: (a) positive electrode potential, (b) negative electrode potential, (c) cell voltage, and (d) coulombic efficiency measured at 4, 10, 20, 40, 60, 80, and 100C rates (or current densities of 0.24, 0.59, 1.17, 2.35, 3.53, 4.70 and 5.87 mA cm^{-2}).

the final potential decreased from *ca.* 0.83 to 0.71 V from 4 to 100C, retaining 86% of its initial value at 100C, which was inferior to that of the SSAB-PPNQ cell. The CE of the SSAB-PPNQ cell decreased from 84% to 81% from 4 to 100C (Fig. 3d), which was lower than those of the SSAB-NQ and SSAB-PE-AQ cells (100% to 91% and 96% to 93%, respectively, when operated at 100% RH).

The SSAB-PPNQ cell was charged and discharged at a constant current density of 0.88 mA cm^{-2} (or 15C rate) at 80% RH for 100 cycles, with a restart every 20 cycles, and the charging/discharging curves are presented for every 10 cycles (Fig. 4a–c). Although the charging/discharging curves of the electrodes and cell (Fig. 4a–c) in the 1st cycle were similar to those obtained at a lower current density (0.23 mA cm^{-2} or 3.9C rate, Fig. 2), the overpotentials at both electrodes were slightly higher, resulting in slightly lower charge and discharge capacities of 67.0 and 57.6 mAh g^{-1} respectively (*vs.* 74.4 and 63.1 mAh g^{-1}, respectively, in Fig. 2). The rate characteristics are discussed in more detail above. During the initial four cycles, the charge and discharge capacities gradually decreased from 67.0 and 57.6 mAh g^{-1} to 62.8 and 58.7 mAh g^{-1} from the 1st to the 4th cycles, respectively (Fig. S7†). Thereafter, the charging/discharging curves remained nearly unchanged for up to 100 cycles, indicating the excellent cycling stability of the SSAB-PPNQ cell. In the 100th cycle, the charge and discharge capacities were 61.3 and 57.5 mAh g^{-1}, respectively, accounting for 98% remaining compared to those of the 4th cycle (Fig. 4d). The CE of the SSAB-PPNQ cell remained nearly constant, at 93% over 100 cycles, which was slightly lower than that of the SSAB-NQ cell (>98% over 100 cycles at 100% RH). Nevertheless, the SSAB-PPNQ cell exhibited superior cycle stability compared to the SSAB-NQ cell, as the discharge capacity of the latter declined from 81.7 to 73.6 mAh g^{-1} over 100 cycles, with *ca.* 90% retention of its discharge capacity. The improved stability of the SSAB-PPNQ cell in both rate performance and cycling test (as summarized in Table S3†) compared to the SSAB-NQ cell was partly attributable to the polymeric structure of PPNQ, which stabilized the negative electrode without dissolution and/or decomposition. The CV curve of the negative electrode after 100 cycles was nearly identical to that of the pristine one, with a slightly higher redox-active material utilization (18% *vs.* 17%) (Fig. 4e), further proving the excellent stability of PPNQ in the electrode. However, a sharp peak was observed at *ca.* −0.1 V in the cycled CV curve in the negative-going scan, indicating that the HER was more likely to occur in the aged electrode.[14] The EIS spectrum (Fig. S4†) of the cycled SSAB-PPNQ cell showed only a slightly lower Z' value (*ca.* 1.13 Ω) compared to the pristine cell (*ca.* 1.16 Ω), confirming the electrochemical stability of the electrode components. The cycled SSAB-PPNQ cell under fully humidified conditions (100% RH) demonstrated a more pronounced redox peak in the CV curve and higher redox-active material utilization compared to operation at 80% RH (20% *vs.* 18%) (Fig. S8†). The charging/discharging

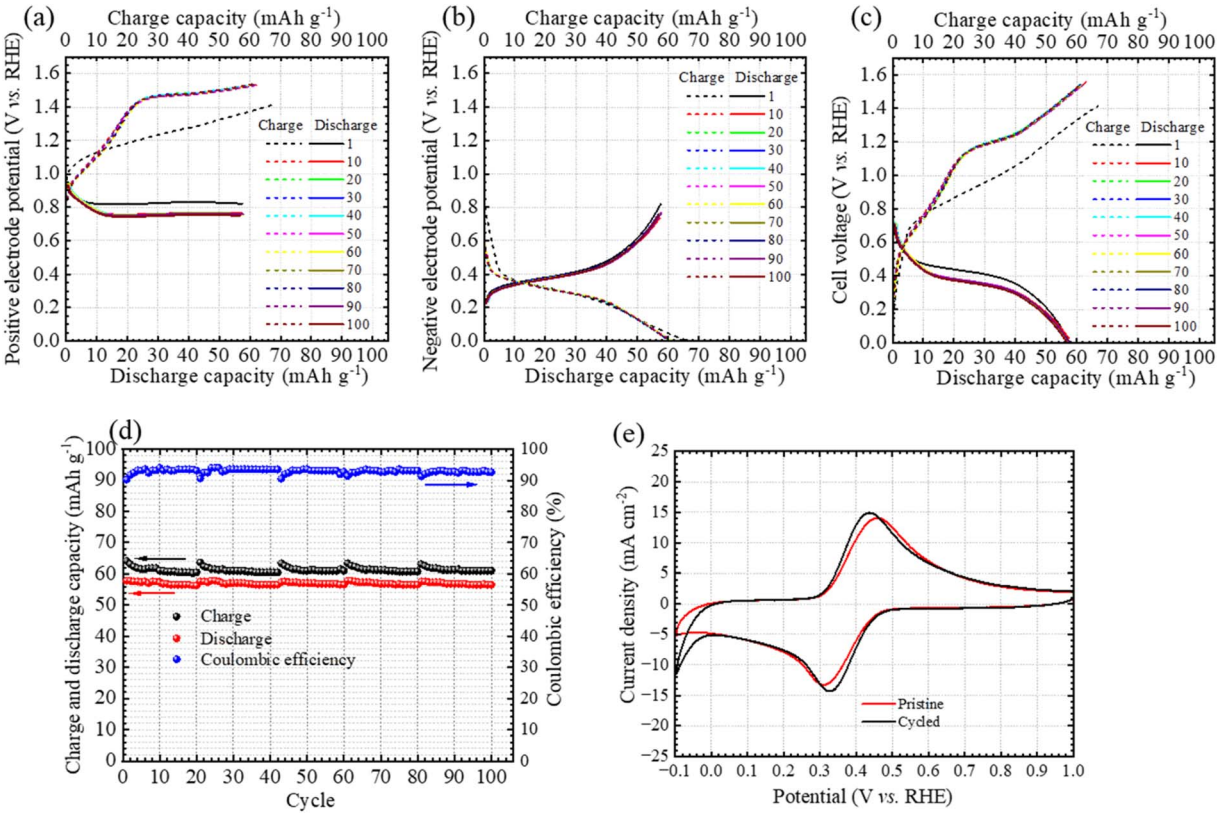

Fig. 4 Charging/discharging curves of the SSAB-PPNQ cell measured during cycling at 0.88 mA cm^{-2} (at a 15C rate): (a) positive electrode potential, (b) negative electrode potential, and (c) cell voltage. Changes in (d) charge/discharge capacities and coulombic efficiencies during cycling. (e) CV curves scanned at 20 mV s^{-1} for pristine and cycled negative electrodes.

curves at 100% RH remained similar to those at 80% RH, and the charge and discharge capacities were higher, *ca.* 90 and 72 mAh g^{-1} at 0.23 mA cm^{-2} (at a 3.4C rate) (Fig. S9†) and 68 and 64 mAh g^{-1} at 1.02 mA cm^{-2} (at a 15C rate) (Fig. S10†), respectively, suggesting enhanced capacity at higher humidity. The charging/discharging curves were stable over 10 cycles. The aged CCM recovered from the cell was analyzed by SEM to examine the cross-sectional morphologies of the positive and negative electrodes (Fig. S2d–f†). The images revealed that the morphology and thickness of both electrodes remained unchanged and nearly identical to those of the fresh CCM with no evidence of particle aggregation, indicating stability of the electrode components during the cycle test.

Conclusion

We successfully synthesized a novel redox-active NQ-based polymer, PPNQ, and evaluated its electrochemical properties when used as the negative electrode material in an SSAB. To the best of our knowledge, this represents the first demonstration of a polymeric NQ-based material integrated into an all-solid-state air battery system. Compared to previously examined small organic molecules, such as NQ, polymeric PPNQ exhibited enhanced affinity for the hydrophilic proton-conductive polymer (Nafion™), facilitating proton transport and leading to higher redox-active material utilization, thereby improving the capacitive performance of the SSAB-PPNQ cell. Furthermore, PPNQ functioned more stably in the electrode than other materials, demonstrating reduced dissolution and/or possible degradation during repeated charge/discharge cycles, which enhanced the rate properties (84% retention of its discharge capacity at 100C) and cyclability (98% retention of its charge/discharge capacities over 100 cycles) of the SSAB-PPNQ cell. This stable performance under high-rate and long-term cycling conditions is particularly notable for an organic polymer in all-solid-state battery configurations. These findings highlight the promising electrochemical performance of PPNQ under reduced humidity conditions and present a new molecular design strategy for organic electrode materials that enables both high stability and excellent redox reversibility. They also underscore the potential of redox-active polymers as efficient and durable electrode materials for high-performance SSABs.

Data availability

The data supporting this article has been included as part of the ESI.†

Author contributions

Lin Guo: investigation and writing. Kenji Miyatake: supervision, writing, reviewing and editing, funding acquisition, and project

administration. Fang Xian: reviewing. Fanghua Liu: reviewing. Ahmed Mohamed Ahmed Mahmoud: reviewing. Vikrant Yadav: reviewing. Chun Yik Wong: reviewing.

Conflicts of interest

There are no conflicts of interest to declare.

Acknowledgements

This work was partly supported by the Ministry of Education, Culture, Sports, Science and Technology (MEXT), Japan, through Grants-in-Aid for Scientific Research (23H02058) and the MEXT Program: Data Creation and Utilization Type Material Research and Development Project (JPMXP1122712807), the Toshiaki Ogasawara Memorial Foundation, and JKA promotion funds from AUTORACE.

References

1 Q. Sun, L. Dai, T. Luo, L. Wang, F. Liang and S. Liu, *Carbon Energy*, 2023, **5**, e276.
2 Y. Sun, *ACS Energy Lett.*, 2020, **5**, 3221–3223.
3 H. Wan, Z. Wang, W. Zhang, X. He and C. Wang, *Nature*, 2023, **623**, 739–744.
4 J. Sung, J. Heo, D. Kim, S. Jo, Y. Ha, D. Kim, S. Ahn and J. Park, *Mater. Chem. Front.*, 2024, **8**, 1861–1887.
5 G. Cong, W. Wag, N. Lai, Z. Liang and Y. Lu, *Nat. Mater.*, 2019, **18**, 390–396.
6 P. Leung, D. Aili, Q. Xu, A. Rodchanarowand and A. A. Shah, *Sustainable Energy Fuels*, 2018, **2**, 2252–2259.
7 S. Li, S. Hu, H. Li and C. Han, *Angew. Chem., Int. Ed.*, 2024, **63**, e202318885.
8 K. Oka, S. Murao, M. Kataoka, H. Nishide and K. Oyaizu, *Macromolecules*, 2021, **54**, 4854–4859.
9 L. Zhong, Z. Fang, C. Shu, C. Mo, X. Chen and D. Yu, *Angew. Chem., Int. Ed.*, 2021, **60**, 10164–10171.
10 M. Yonenaga, Y. Kaiwa, K. Oka, K. Oyaizu and K. Miyatake, *Angew. Chem., Int. Ed.*, 2023, **62**, e202304366.
11 K. Miyatake, S. Wada, L. Guo, F. Xian, F. Liu, A. M. A. Mahmoud, V. Yadav and C. Y. Wong, *Energy Environ. Mater.*, 2025, **8**, e12887.
12 L. Zhao, Y. Li, M. Yu, Y. Peng and F. Ran, *Adv. Sci.*, 2023, **10**, 2300283.
13 L. Guo, K. Miyatake, S. Wada, K. Oka, S. Kitajima, H. Kasai, R. Tanaka, H. Imoto, K. Naka, F. Xian, F. Liu, A. Mohamed Ahmed Mahmoud, V. Yadav and C. Y. Wong, *ACS Sustainable Chem. Eng.*, 2024, **12**, 16518–16523.
14 A. Rana, K. Roy, J. N. Heil, J. H. Nguyen, C. Renault, B. M. Tackett and J. E. Dick, *Adv. Energy Mater.*, 2024, **14**, 2402521.

